



Cite this: *Phys. Chem. Chem. Phys.*, 2015, 17, 3617

A kinetic study of the CH_2OO Criegee intermediate self-reaction, reaction with SO_2 and unimolecular reaction using cavity ring-down spectroscopy[†]

Rabi Chhantyal-Pun,^a Anthony Davey,^a Dudley E. Shallcross,^a Carl J. Percival^b and Andrew J. Orr-Ewing^{*a}

Criegee intermediates are important species formed during the ozonolysis of alkenes. Reaction of stabilized Criegee intermediates with various species like SO_2 and NO_2 may contribute significantly to tropospheric chemistry. In the laboratory, self-reaction can be an important loss pathway for Criegee intermediates and thus needs to be characterized to obtain accurate bimolecular reaction rate coefficients. Cavity ring-down spectroscopy was used to perform kinetic measurements for various reactions of CH_2OO at 293 K and under low pressure (7 to 30 Torr) conditions. For the reaction $\text{CH}_2\text{OO} + \text{CH}_2\text{OO}$ (8), a rate coefficient $k_8 = (7.35 \pm 0.63) \times 10^{-11} \text{ cm}^3 \text{ molecule}^{-1} \text{ s}^{-1}$ was derived from the measured CH_2OO decay rates, using an absorption cross section value reported previously. A rate coefficient of $k_4 = (3.80 \pm 0.04) \times 10^{-11} \text{ cm}^3 \text{ molecule}^{-1} \text{ s}^{-1}$ was obtained for the $\text{CH}_2\text{OO} + \text{SO}_2$ (4) reaction. An upper limit for the unimolecular CH_2OO loss rate coefficient of $11.6 \pm 8.0 \text{ s}^{-1}$ was deduced from studies of reaction (4). SO_2 catalysed CH_2OO isomerization or intersystem crossing is proposed to occur with a rate coefficient of $(3.53 \pm 0.32) \times 10^{-11} \text{ cm}^3 \text{ molecule}^{-1} \text{ s}^{-1}$.

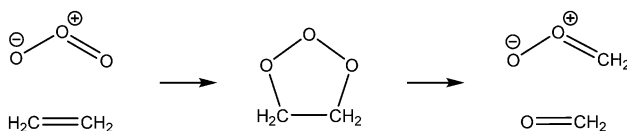
Received 18th September 2014,
Accepted 22nd December 2014

DOI: 10.1039/c4cp04198d

www.rsc.org/pccp

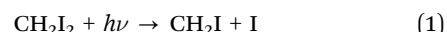
Introduction

In 1949 Rudolph Criegee¹ proposed that an intermediate (later to be called a Criegee intermediate) was formed during the ozonolysis of alkenes. On addition of ozone to an alkene a primary ozonide (POZ) is formed which decomposes to form a carbonyl and a Criegee intermediate (CI).^{2–4} Taking ethene as an example, the following reaction sequence leads to the formation of the simplest CI, CH_2OO .



The Criegee intermediate formed can undergo rapid unimolecular decomposition, often to yield OH radicals,^{5–7} but a second much slower decomposition has been observed and attributed to so called stabilised CI (SCI).^{6,7} These SCI are formed with internal

energies below the threshold to unimolecular decomposition and are sufficiently long lived to undergo reaction with atmospheric trace gases. SCIs were postulated but remained undetected in the gas-phase until the work of Taatjes and co-workers,^{8–12} who showed that these SCIs could be generated through photolysis of alkyl diiodide species in the presence of oxygen, *e.g.*



This breakthrough has led to many recent studies that have investigated the UV/visible,^{13–19} IR^{20,21} and microwave^{22–24} spectra, as well as several kinetic studies of CH_2OO and CH_3CHO with SO_2 , NO , NO_2 , carbonyls, alkenes and organic acids.^{8–11,16,25–30} Direct studies, *i.e.* ones that monitor the decay of SCI or a proxy of the SCI (*e.g.* HCHO , OH) return rate coefficients that are considerably larger than previous indirect estimates based on end product analysis.² These new kinetic data suggest a greater role for SCI species in the atmospheric oxidation of SO_2 and NO_2 in particular.

Field measurements support a role for the SCI assisted production of H_2SO_4 (ref. 31) and although model studies disagree as to the extent, they do agree that there is a non-negligible impact of CIs on oxidation of SO_2 .^{32–34} If the gas-phase

^a School of Chemistry, University of Bristol, Cantock's Close, Bristol, BS8 1TS, UK.
E-mail: a.orr-ewing@bristol.ac.uk

^b Centre for Atmospheric Science, School of Earth, Atmospheric and Environmental Sciences, University of Manchester, Simon Building, Oxford Road, Manchester, M13 9PL, UK

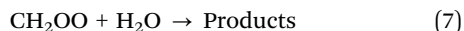
† Electronic supplementary information (ESI) available. See DOI: 10.1039/c4cp04198d



oxidation of SO_2 to SO_3 (and subsequently H_2SO_4) by SCI competes with, or even dominates in regions of the lower troposphere, over the oxidation by OH, the formation of H_2SO_4 may be accelerated and aerosol nucleation rates affected.^{32,33}

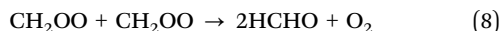


There is considerable debate concerning the impact of these new data, with models predicting effects ranging from significant through to more modest. Given the differences in chemical scheme used in these various model studies as well as model resolution, current disagreement on SCI impact remains to be resolved. However, models that contain detailed chemistries, *e.g.* the Master Chemical Mechanism³² and its surrogate the Common Representative Intermediates scheme,³³ return a more significant impact than those models with less hydrocarbon chemistry.³⁴ A major issue at the core of these discrepancies concerns the two loss processes that dominate the SCI concentration, unimolecular loss and reaction with water vapour:



Welz *et al.*, Li *et al.*, and Percival *et al.* noted that significant SCI levels are predicted if k_6 is around 200 s^{-1} or less and if k_7 is less than around $1 \times 10^{-16} \text{ cm}^3 \text{ molecule}^{-1} \text{ s}^{-1}$.^{9,32,33} Further work is required to determine k_6 and k_7 more accurately.

Recent work has shown that the rate coefficient for the self-reaction of CH_2OO (reaction (8)) is very large.³⁵



Although this reaction has no atmospheric relevance, it could be important in laboratory studies that probe the kinetics and mechanisms of alkene ozonolysis.³⁶ In this paper we report measurements of k_4 , k_6 and k_8 at room temperature over a range of pressure, using near UV cavity ring-down spectroscopy (CRDS) to detect CH_2OO . Where appropriate, we compare with previously reported rate coefficients obtained using alternative methods.

Experimental

Cavity ring down spectroscopy was used to probe temporal profiles of CH_2OO signals in flowing gas samples using the known $\tilde{\text{B}}(^1\text{A}') \leftarrow \tilde{\text{X}}(^1\text{A}')$ electronic absorption band in the near ultraviolet (UV) spectral region. UV probe radiation was generated by frequency doubling the visible radiation output of a dye laser (Sirah CobraStretch, with pyridine 1 dye) pumped by the second harmonic of a Nd:YAG laser (Continuum Surelite III-10). A probe wavelength of 355 nm was chosen to maximize CH_2OO absorption^{13,16} and minimize interferences. The ESI† provides detailed discussion of possible interferences and their elimination.

The third harmonic of a Continuum Surelite I-10 Nd:YAG laser ($\lambda = 355 \text{ nm}$; 100 mJ per pulse; energy density $\sim 500 \text{ mJ cm}^{-2}$, $<10 \text{ ns}$ pulse duration) was used to photolyze CH_2I_2 to start the chemistry leading to production of CH_2OO . The unfocussed

photolysis beam had a diameter of 5 mm with a top-hat intensity profile, and crossed the probe beam (with beam waist of 0.24 mm) at an angle of 5°, giving an overlap length of 5.7 cm in the centre of the CRDS cavity. The delay between the two laser pulses was controlled by a BNC 555 digital delay generator.

High reflectivity mirrors ($R > 99.9\%$ at 355 nm, 100 cm radius of curvature) were mounted 106 cm apart at opposite ends of a glass tube to form the ring-down cavity. Light escaping from one end mirror of the cavity was monitored by a photodiode (New Focus 1801) and digitized by an 8 bit oscilloscope (LeCroy Waverunner 6030; 350 MHz, 2.5 GSamples per s). Typical ring-down times $<6 \mu\text{s}$ were much shorter than the 1–10 ms timescales used for reaction kinetics measurements under our experimental conditions.

The 6 cm diameter glass tube confined the flow of reagent and bath gases along the detection axis of the spectrometer. The flow rates for all gases were regulated by calibrated mass flow controllers (MKS 1479A and 1179A). The precursor molecule, diiodomethane (CH_2I_2 , 99%), and sulphur dioxide (SO_2 , $\geq 99.9\%$) were purchased from Sigma-Aldrich. CH_2I_2 was purified further by freeze-pump-thaw cycling before use. High purity nitrogen (N_2) and oxygen (O_2) were obtained from Air Liquide. Pre-mixtures of CH_2I_2 in N_2 (0.7 Torr/750 Torr) and SO_2 in N_2 (5 or 750 Torr/1500 Torr) were made and allowed to mix for at least a day to obtain a homogenous mixture. Low flows (20 sccm) of nitrogen were passed through purge lines close to the ring down mirrors to prevent mirror contamination. All the other gases were passed into the flow tube through a port close to the centre of the cavity. 1.0 to 2.0 Torr of the precursor premixes, 1.0 Torr of oxygen and various pressures of nitrogen were used for the experiments. Sample pressures were measured by two capacitance manometers (0–10 Torr and 0–1000 Torr) located close to the centre of the flow tube. Total flow rates (excluding the mirror purges) ranged from 50–500 sccm, and we verified that the purge flows did not significantly change the overall column length of the gas mixture used in kinetic studies over the total pressure range 7–30 Torr by measuring absorption by CH_2I_2 or added NO_2 . We obtained average gas sample lengths of $37 \pm 3 \text{ cm}$ that are a factor of 6.5 longer than the overlap region of the photolysis and probe laser beams in which the chemistry of interest occurs. The arrangement of the overlap of the probe and much-larger diameter photolysis laser beams gives a flat concentration profile across the probe region at early times, and diffusion out of the probe volume is expected to be a first order process. We also calculate that mass flow across the probe volume will have negligible effects over the timescales of our kinetic measurements.

Further details of the spectrometer and optimization of experimental conditions are provided in the ESI.†

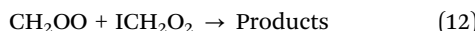
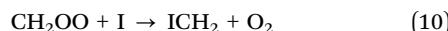
Results and discussion

(I) $\text{CH}_2\text{OO} + \text{CH}_2\text{OO}$ reaction

Relatively high concentrations of CH_2OO need to be produced in laboratory experiments in order to provide enough signal for kinetic measurements. In the present work, typical initial CH_2OO concentrations of $2.5\text{--}5.0 \times 10^{12} \text{ molecule cm}^{-3}$ were generated. Under such conditions, the self-reaction can contribute



significantly to the overall loss of CH_2OO . Recently, Su *et al.* reported a CH_2OO self-reaction rate constant of $k_8 = (4 \pm 2) \times 10^{-10} \text{ cm}^3 \text{ molecule}^{-1} \text{ s}^{-1}$ by monitoring depletion of infrared bands.³⁵ This value was refined to $k_8 = (6.0 \pm 2.1) \times 10^{-11} \text{ cm}^3 \text{ molecule}^{-1} \text{ s}^{-1}$ by Buras *et al.*, by simultaneous monitoring of the near UV band of CH_2OO and near IR absorption of iodine atoms.³⁷ Recently, Ting *et al.* reported a k_8 value of $(8 \pm 4) \times 10^{-11} \text{ cm}^3 \text{ molecule}^{-1} \text{ s}^{-1}$ using broadband UV absorption spectroscopy and monitoring CH_2OO depletion along with that of CH_2I and IO .³⁸ Reaction of CH_2I with O_2 was used to produce CH_2OO in all of these studies. Using photoionization mass spectrometry, this chemical route was shown to produce sufficient CH_2OO radical concentration to perform kinetic measurements.⁹ In this work we used a similar reaction pathway shown by reactions (1) and (2) to produce CH_2OO . Other than the self-reaction, we also considered the following removal pathways for CH_2OO and I.



Under our experimental conditions, CH_2I is expected to react with O_2 within the first time step (200 μs) of the kinetic measurements. The branching ratio of reactions (2) and (3) determines the yield of CH_2OO which increases with a decrease in the concentration of the third body (M). Under low pressure conditions and in the absence of other reactant species, the self-reaction (8), and reactions (9)–(11) with iodine atoms, are expected to be the major loss mechanism for CH_2OO . At higher pressures, contribution from reaction (12) will increase. Assuming the fast self-reaction to be the dominant loss mechanism, the decay traces of CH_2OO were fitted to an integrated second order decay expression. Further justification for this fitting procedure is provided later. For a second order decay mechanism,

$$\frac{dN}{dt} = -2k_{\text{obs}}N^2 \quad (14)$$

in which k_{obs} is the effective second order decay rate coefficient, t is time and N is the CH_2OO concentration. The integrated second order decay rate expression is

$$N(t) = \frac{N(t_0)}{1 + 2k_{\text{obs}}N(t_0)t} \quad (15)$$

In eqn (15), $N(t_0)$ is the initial CH_2OO concentration. In our cavity ring-down measurements, probe light intensity decay rate constants, κ , (or ring-down times, $\tau = 1/\kappa$) are measured with and without the photolysis laser on to give a transient absorption signal. The concentration of the absorbing species is given by

$$N(t) = \frac{\Delta\kappa(t)L}{cd\sigma_{355\text{nm}}} \quad (16)$$

$$\Delta\kappa = \left(\frac{1}{\tau_{\text{on}}} - \frac{1}{\tau_{\text{off}}} \right) \quad (17)$$

where τ_{on} and τ_{off} are ring down times with the photolysis laser on and off, L is the length of the cavity, c is the speed of light, $d = 5.7 \text{ cm}$ is the photolysis and probe laser overlap length, $\sigma_{355\text{nm}}$ is the absorption cross-section of CH_2OO at the probe wavelength 355 nm and the change in ring-down rate, $\Delta\kappa$, is directly proportional to the CH_2OO concentration. Characterization of the overlap length is presented in the ESI.† Combining eqn (15) and (16) gives

$$\Delta\kappa(t) = \frac{1}{\frac{1}{\Delta\kappa(t_0)} + \left(\frac{2L}{cd} \right) k't} \quad (18)$$

$$k' = \frac{k_{\text{obs}}}{\sigma_{355\text{nm}}} \quad (19)$$

where k' is the observed second order decay rate coefficient scaled with respect to the CH_2OO absorption cross section at 355 nm. Uncertainty in the absorption cross section of CH_2OO at the probe wavelength determines the uncertainty in the k_{obs} value, and as such a cross-section independent value is desired. Thus, the effective second order decay coefficient is expressed in terms of k' , which can be readily converted to a second-order rate coefficient for a given choice of value for $\sigma_{355\text{nm}}$.

The ESI† summarizes possible sources of interferences at the 355 nm probe wavelength and our procedure for their elimination. The interference-subtracted decay traces were fitted to eqn (18) as exemplified by the data shown in Fig. 1. Data points starting from a 200 μs time delay to around 10 ms were included in the fit. Reaction (2) is calculated to have a half-life of 11.8 μs based on the bimolecular rate coefficient of $1.82 \times 10^{-12} \text{ cm}^3 \text{ molecule}^{-1} \text{ s}^{-1}$ (ref. 16) and hence is expected to be complete by 200 μs . Experimental conditions were selected such that the CH_2OO signal depletes by greater than 90% by a photolysis-probe delay of 10 ms. Under such conditions, non-second order loss mechanisms like diffusion and mass flow do not contribute significantly to the decay mechanism, as discussed in the Experimental section. Details of the experiments to characterize the non-second order loss mechanisms in the detection region of the flow tube are presented in the ESI.†

CH_2OO decay traces were obtained for different initial concentrations of the CH_2OO (see ESI†) and at different bath gas (N_2) pressures. Fig. 2 shows the fitted k' values obtained from kinetic decay traces as a function of the bath gas concentration. These values are also provided in Table S4 in the ESI.† The quality of the second order fits for the CH_2OO decay traces under all the pressure conditions (7 to 30 Torr) is excellent, with adjusted R^2 values greater than 0.99. A second order decay form of the type used in the analysis is strictly valid for a bimolecular reaction in which the two reactants are of equal concentrations. Thus, the extracted k' values should derive primarily from the self-reaction of CH_2OO or reaction of CH_2OO with similar concentrations of other molecules like ICH_2O_2 , I atom or a mixture of both. The obtained values show a positive

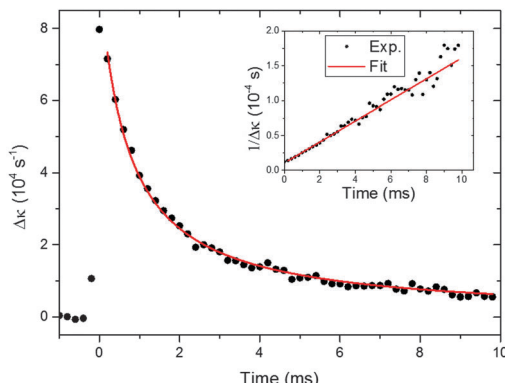


Fig. 1 Time-dependent CH_2OO intermediates signal under conditions in which the self-reaction (8) dominates. Black circles show the experimental CH_2OO signal and the red line is a fit of the experimental signals to eqn (18). The initial CH_2OO concentration was $\sim 5.1 \times 10^{12}$ molecule cm^{-3} . The inset shows the reciprocal of the experimental and fitted $\Delta\kappa$ values as a function of time for clarity.

dependence on N_2 bath gas pressure. The I atom yield is expected to decrease with increasing pressure, whereas the contribution from the reaction between ICH_2OO and CH_2OO should increase with an increase in pressure. The CH_2OO self-reaction rate coefficient has been calculated to be independent of pressure.^{30,35} The pressure range studied in the current work offers a window in which the concentrations of CH_2OO and of co-reactants, either ICH_2OO or I atoms, are such that the overall CH_2OO decay follows a second order form. The relative contributions of these reactions to the value of k' are discussed later.

An empirical linear fit was performed for the plot of k' values as a function of N_2 concentration as shown in Fig. 2. The quality of the fit is good, with an adjusted R^2 value greater than 0.99, and the intercept was taken as the zero pressure limit value for k' . The rate of reaction (9) should decrease with a decrease in the third body concentration, which lowers the yield of ICH_2OO , whereas the rate coefficients for (10) and (11) are calculated to be independent of pressure³⁵ and could contribute significantly to the CH_2OO loss along with the dominant self-reaction under low pressure conditions. A quantitative analysis

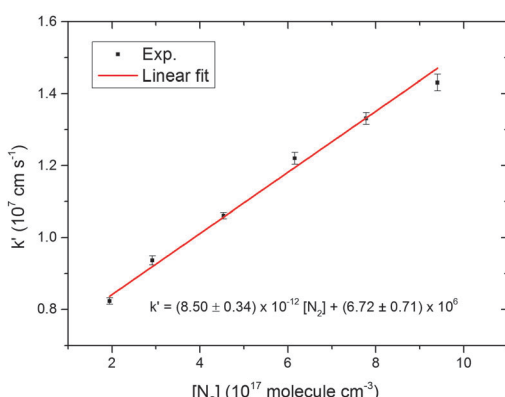


Fig. 2 CH_2OO overall scaled second order decay rate coefficient, k' , as a function of N_2 concentration. The error bars are the 1σ uncertainties from the fits of kinetic decay traces such as that shown in Fig. 1 to eqn (18).

of the pressure dependence evident in Fig. 2 is presented in the ESI,[†] and our observations can be accounted for if the rate coefficient for reaction of CH_2OO with ICH_2OO is $k_{12} \approx 2 \times 10^{-10}$ cm^3 molecule⁻¹ s^{-1} . This value is consistent with the rate coefficient for $\text{CH}_2\text{OO} + \text{HO}_2$ of $k = 2.23 \times 10^{-10}$ cm^3 molecule⁻¹ s^{-1} calculated by Long *et al.*³⁹ and is a factor of ~ 4 lower than the limiting capture rate for a barrierless reaction that we predict from estimated dipole moments for CH_2OO and ICH_2OO .

The zero pressure limit value for k' can therefore be taken as an upper limit for the CH_2OO self-reaction rate coefficient k_8 scaled by $\sigma_{355\text{nm}}$ (eqn (19)). Table 1 shows the k_{obs} values obtained by using the zero pressure limit k' value and the $\sigma_{355\text{nm}}$ values reported by various sources. The CH_2OO $\sigma_{355\text{nm}}$ value from the work of Ting *et al.* is expected to be the most accurate as the CH_2OO $\sigma_{375\text{nm}}$ value reported in their study is similar to the value obtained by Buras *et al.* using a different method. Thus, with incorporation of the quoted uncertainty for $\sigma_{355\text{nm}}$ values, $k_8 \leq 7.98 \times 10^{-11}$ cm^3 molecule⁻¹ s^{-1} is the best estimate for the self-reaction rate coefficient of CH_2OO from this empirical approach.

To estimate the contributions from reactions (10) and (11) to the value of k_{obs} , numerical kinetic fits were performed for the 7 Torr total pressure CH_2OO decay trace. This chosen decay trace should have minimum contribution from the pressure dependent reactions. The I atom self-reaction, (13), $\text{CH}_2\text{OO} + \text{I}$ reaction and the CH_2OO self-reaction, (8), were used in the model for the numerical fit. The $\text{CH}_2\text{OO} + \text{I}$ reaction takes into account the combined effects from reactions (10) and (11) and k_{Iodine} is taken as its overall rate coefficient. The initial I atom concentration was fixed to twice the CH_2OO concentration and a rate coefficient value of 2.83×10^{-15} cm^3 molecule⁻¹ s^{-1} was used for reaction (13), obtained using a kinetic rate coefficient expression ($M = \text{N}_2 = 7$ Torr, $T = 298$ K) reported previously.⁴⁰ Fig. 3 shows the results of the fits obtained by varying the k_{Iodine} values while floating the k_8 values. No significant contribution from k_{Iodine} was found as the fits obtained with the k_{Iodine} value floated and with no contribution from the $\text{CH}_2\text{OO} + \text{I}$ reaction (*i.e.* $k_{\text{Iodine}} = 0$ cm^3 molecule⁻¹ s^{-1}) were identical. The k_{Iodine} value could not be determined from these fits because the dominant removal process for CH_2OO is self-reaction ($k_8 \gg k_{\text{Iodine}}$) under our conditions. The fits obtained by using k_{Iodine} values of 0.5 and 1.0×10^{-11} cm^3 molecule⁻¹ s^{-1} are of significantly lower quality, consistent with the observations of Buras *et al.* The k_8 values obtained from these different fits are listed in Table 2.

Table 1 Effective second order decay rate coefficient, $k' = k_{\text{obs}}/\sigma_{355\text{nm}}$, for the loss of CH_2OO at the low pressure limit. The values of k_{obs} reported in the fourth column are obtained using $\sigma_{355\text{nm}}$ values from various sources

$k' (10^6 \text{ cm s}^{-1})$	$\sigma_{355\text{nm}} (10^{-17} \text{ cm}^2 \text{ molecule}^{-1})$	$\sigma_{355\text{nm}}$ source	$k_{\text{obs}} (10^{-11} \text{ cm}^3 \text{ molecule}^{-1} \text{ s}^{-1})$
6.72 ± 0.17	1.13 ± 0.05	Ting <i>et al.</i> ¹⁸	7.59 ± 0.39
	2.5^a	Beames <i>et al.</i> ¹³	16.8^a
	3.6 ± 0.9	Sheps ¹⁶	24.2 ± 6.1

^a The value of $\sigma_{355\text{nm}}$ (with uncertainty on the order of a factor of 2) was obtained from a Gaussian fit to the spectrum reported by Beames *et al.*



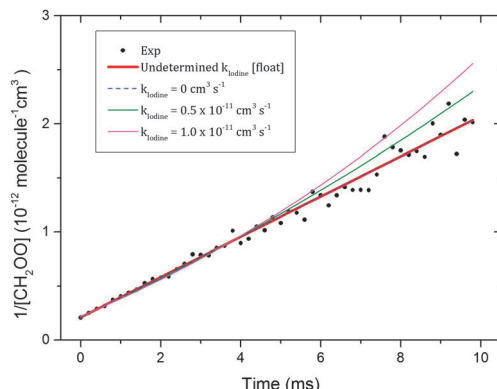


Fig. 3 Numerical kinetic fits for the 7 Torr pressure CH_2OO decay trace using various k_{Iodine} values. The CH_2OO concentration was obtained using the $\sigma_{355\text{nm}}$ value reported by Ting *et al.* and the initial CH_2OO concentration was $\sim 4.7 \times 10^{12}$ molecule cm^{-3} .

Table 2 Values for the CH_2OO self-reaction obtained from the numerical kinetic fits for different values of k_{Iodine} as shown in Fig. 3

$k_{\text{Iodine}} (10^{-11} \text{ cm}^3 \text{ molecule}^{-1} \text{ s}^{-1})$	$k_8 (10^{-11} \text{ cm}^3 \text{ molecule}^{-1} \text{ s}^{-1})$
0.00 ^a	9.30 ± 0.09^a
0.00	9.30 ± 0.09
0.50	8.00 ± 0.11
1.00	6.85 ± 0.13

^a Both k_{Iodine} and k_8 were floated in the fit.

Taking $1.0 \times 10^{-11} \text{ cm}^3 \text{ molecule}^{-1} \text{ s}^{-1}$ as a conservative upper limit estimate for k_{Iodine} , the fitted k_8 value $(6.85 \pm 0.13) \times 10^{-11} \text{ cm}^3 \text{ molecule}^{-1} \text{ s}^{-1}$ is taken as a lower limit. Combining this lower limit estimate with the upper limit estimate from the empirical analysis and propagating the uncertainties, a value of $(7.35 \pm 0.63) \times 10^{-11} \text{ cm}^3 \text{ molecule}^{-1} \text{ s}^{-1}$ is obtained as the best estimate for k_8 in the current work.

The k_8 value obtained from the current work is compared with ones reported previously in Table 3. Our k_8 value is well within the bounds of uncertainty of the value reported by Buras *et al.*³⁷ Both of these values are significantly lower than the one reported by Su *et al.*³⁵ Although the k_8 values from this work and the work of Buras *et al.* agree well, the analyses performed are quite different. Their kinetic study was performed by monitoring absorbance of CH_2OO and I atoms. A kinetic model was used to obtain the upper limit for the $\text{CH}_2\text{OO} + \text{I}$ rate coefficient that simultaneously fitted I atom and CH_2OO decay traces, taking into account self-reactions, unimolecular losses, and cross-reactions. However, a simpler model showed that the $\text{CH}_2\text{OO} + \text{I}$ reaction is in the pseudo first order limit, and the overall loss of CH_2OO signal results from contributions from the CH_2OO self-reaction and this pseudo first order reaction of CH_2OO and I. Both of these approaches led Buras *et al.* to suggest a maximum rate coefficient value of $1 \times 10^{-11} \text{ cm}^3 \text{ molecule}^{-1} \text{ s}^{-1}$ for the overall reaction of I atom with CH_2OO , so the self-reaction dominates. The yields for both I atom and CH_2OO increase with a decrease in pressure, and thus the pseudo first order contribution of the $\text{CH}_2\text{OO} + \text{I}$

Table 3 Comparison of CH_2OO self-reaction rate coefficients, k_8 , obtained from the current work with previously reported values. Uncertainties incorporate both those from our measurements of $k_8/\sigma_{355\text{nm}}$ and the reported uncertainties in $\sigma_{355\text{nm}}$

$k_8 (10^{-11} \text{ cm}^3 \text{ molecule}^{-1} \text{ s}^{-1})$	Source
7.35 ± 0.63	This work
6.0 ± 2.1	Buras <i>et al.</i> ³⁷
40 ± 20	Su <i>et al.</i> ³⁵
8 ± 4	Ting <i>et al.</i> ³⁸

reaction to the overall CH_2OO decay is expected to be either similar, or perhaps larger, in the pressure range used in the current work. However, the CH_2OO decay profiles obtained in the current study are predominantly second order. Contrary to the observations of Buras *et al.*, we see a definite increase in the effective second order rate coefficient value with pressure, most likely because of contributions from reactions (9) and (12) (see above, and ESI†). These contributions, instead of the $\text{CH}_2\text{OO} + \text{I}$ reaction, might cause the decay of CH_2OO to assume first-order behaviour with further increase in pressure, and could explain the observations of purely second order CH_2OO decay in the current work and the combined first and second order decays of Buras *et al.* Nevertheless, both approaches should be equivalent in principle to separate the contributions from the self-reaction and other reactions of CH_2OO .

Inclusion of the CH_2OO self-reaction could be important in the kinetic models for analysis of the end-products of alkene-ozonolysis reactions used to determine the consequences of Criegee intermediate chemistry in the atmosphere. However, the scope of the current work is to obtain bimolecular reaction rate coefficients for the reaction of CH_2OO with atmospherically relevant species and inclusion of the overall second order loss of CH_2OO in kinetic analysis schemes should suffice. Further detailed discussion of the contribution of the second order loss of CH_2OO in the presence of other reagents is presented in the ESI.† Inclusion of the second order loss mechanism will be especially important to characterize accurately the small, but atmospherically relevant, rate coefficients for reactions of CI with species like H_2O . Also, in the $\text{CH}_2\text{I}_2 + \text{O}_2$ synthesis method, the CH_2OO second order loss contribution increases with pressure as shown in Fig. 2, and thus should be included in the analysis of experimental results obtained at higher pressures.

(II) $\text{CH}_2\text{OO} + \text{SO}_2$ reaction

CH_2OO oxidizes SO_2 to SO_3 (reaction (4)) and hence may contribute to atmospheric sulphuric acid production. The bimolecular reaction rate of $\text{CH}_2\text{OO} + \text{SO}_2$ has been characterized extensively under low pressure and ambient temperature conditions *via* direct and indirect studies. These reaction rate coefficients have been used to verify the presence of CH_2OO and to obtain its near-UV absorption spectrum.¹⁶ However, direct studies at atmospherically relevant pressures and temperatures are still lacking. This section presents some preliminary work on the effect of extending the pressure range and the inclusion of the self-reaction in the analysis to obtain the reaction rate coefficient of CH_2OO with SO_2 using the



direct method. It also explores a possible catalytic isomerization or intersystem crossing (ISC) of CH_2OO in the presence of low concentrations of SO_2 that is proposed to account for some of our experimental observations.

CH_2OO decay traces obtained in the presence of SO_2 are expected to have contributions from both first and second order loss mechanisms

$$\frac{dN}{dt} = -2k_{\text{obs}}N^2 - k_{\text{pseudo}}N \quad (20)$$

here, k_{pseudo} is the pseudo first order rate constant for reaction of CH_2OO with SO_2 which is present in excess. This rate coefficient can, in principle, also contain contributions from mass flow and diffusion, though these are considered small on the ≤ 1 ms timescale of the measurements reported below (see ESI[†]). The second order contribution is provided by bimolecular reactions of CH_2OO , reactions (8), (10) and (11), the overall rate coefficient for which was obtained in the previous section. Eqn (20) is a simple form of Bernoulli's differential equation, the analytical solution for which is provided in ref. 41.

$$N(t) = \frac{k_{\text{pseudo}}N(t_0)}{k_{\text{pseudo}}e^{k_{\text{pseudo}}t} - 2k_{\text{obs}}N(t_0) + 2k_{\text{obs}}N(t_0)e^{k_{\text{pseudo}}t}} \quad (21)$$

combining eqn (16) and (21) gives

$$\Delta\kappa(t) = \frac{k_{\text{pseudo}}}{\frac{k_{\text{pseudo}}}{\Delta\kappa(t_0)}e^{k_{\text{pseudo}}t} - k'\left(\frac{2L}{cd}\right) + k'\left(\frac{2L}{cd}\right)e^{k_{\text{pseudo}}t}} \quad (22)$$

The k' values were fixed to the values obtained from the previous section, whereas $\Delta\kappa(t_0)$ and k_{pseudo} values were floated in the fits. This analysis requires no assumption to be made about the correct value of $\sigma_{355\text{nm}}$. Fig. 4 shows the decays of CH_2OO signal in the presence of different concentrations of SO_2 . The SO_2 concentration range used and the robustness of the pseudo first order approximation are justified in detail in the ESI.[†] These decay traces were fitted to eqn (22) to obtain k_{pseudo} values for each SO_2 concentration. Fig. 5 shows the k_{pseudo} values as a function of SO_2 concentration. The gradient

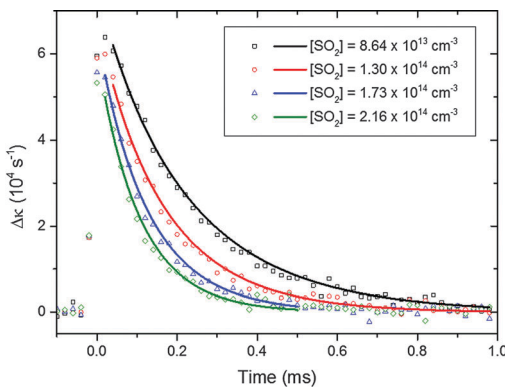


Fig. 4 CH_2OO decay traces in the presence of various concentrations of SO_2 . The initial CH_2OO concentration was $\sim 3.3 \times 10^{12}$ molecule cm^{-3} . All the decay traces were taken at 10 Torr total pressure. Each individual trace was background subtracted using the method described in the ESI.[†] The solid lines show the fits performed using eqn (22).

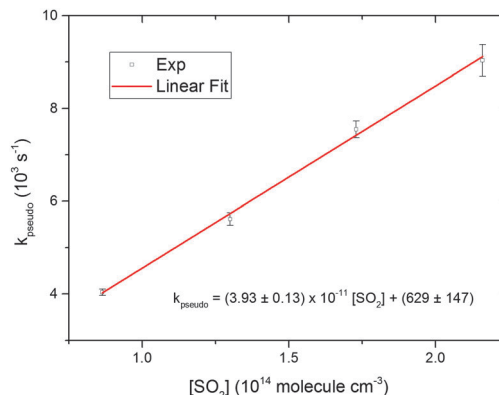


Fig. 5 Linear fit to pseudo first order rate coefficients plotted as a function of SO_2 concentration. The rate coefficients were taken from the fits shown in Fig. 4. The error bars are 1σ value of the individual fits. The uncertainties in the linear fit expression are 1σ values from the fit.

of a linear fit gives the $\text{CH}_2\text{OO} + \text{SO}_2$ bimolecular reaction rate coefficient.

CH_2OO decay traces in the presence of SO_2 were measured for different total pressures in the flow tube. The N_2 pressure was varied while keeping the O_2 (1 Torr) and $\text{CH}_2\text{I}_2\text{-N}_2$ premix (1 Torr) pressures constant to alter the total pressure. Experiments were conducted for several $[\text{SO}_2]$ values to allow pseudo first-order analysis under all total-pressure conditions. Fig. 6 shows the $\text{CH}_2\text{OO} + \text{SO}_2$ bimolecular reaction rate coefficients, k_4 , as a function of total pressure obtained from this work and from previous studies. These values are also provided in Table S4 in the ESI.[†] The k_4 values obtained at different pressures agree within the error of the fits and a pressure independent k_4 value, $(3.80 \pm 0.04) \times 10^{-11}$ cm^3 molecule $^{-1}$ s^{-1} , is obtained by taking an error weighted average. This value is in excellent agreement with the previously reported values^{9,16} also obtained via direct measurement of CH_2OO .

The k_4 values obtained previously at higher pressures via methods monitoring HCHO^{28} or OH^{26} fluorescence show no dependence on pressure, in agreement with the results obtained

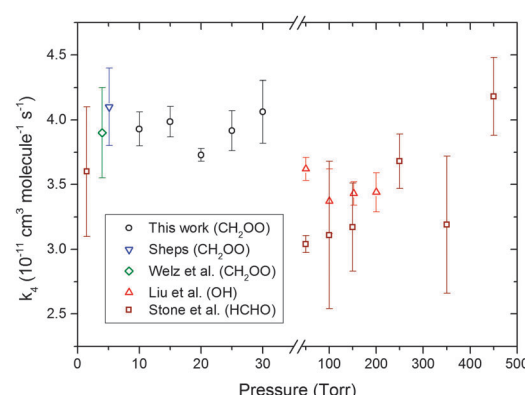


Fig. 6 $\text{CH}_2\text{OO} + \text{SO}_2$ bimolecular reaction rate coefficient as a function of pressure from various sources including the current work. Error bars are 1σ values. The inset key identifies the species monitored in other studies of reaction (4).



in this work for pressures from 10–30 Torr. However, the pressure independent k_4 values obtained in this work and from other CH_2OO loss studies are larger than the ones obtained from the more indirect measurements of HCHO or OH production. In the case of the OH fluorescence experiment, OH radicals can form *via* unimolecular dissociation of CH_2OO , and the k_4 value ($(3.53 \pm 0.29) \times 10^{-11} \text{ cm}^3 \text{ molecule}^{-1} \text{ s}^{-1}$) was obtained from the linear fit of relatively small pseudo first order rate coefficient values (150 to 250 s^{-1}). Under such conditions, contributions from the second order reaction of CH_2OO are significant, and correction for this competing pathway for CH_2OO removal should increase the derived k_4 value.

(III) CH_2OO unimolecular reaction

The unimolecular reaction (6) may be an important loss mechanism for CH_2OO under atmospheric conditions, along with bimolecular reactions with H_2O .³³ No rigorous direct experimental study has been performed so far to obtain a CH_2OO unimolecular decay rate coefficient. Fig. 4 and 5 illustrate the pseudo first order analysis performed to obtain bimolecular rate coefficient for the $\text{CH}_2\text{OO} + \text{SO}_2$ reaction. The intercept value of the linear fit in Fig. 5 should be related to the first order loss of CH_2OO . Unimolecular decay, diffusion and mass flow across the detection axis of the spectrometer could all contribute to the observed first order loss of CH_2OO , but we present evidence in ESI† that the latter two effects are small on the ≤ 1 ms measurement times of these experiments. There should not be significant contribution from wall loss as the radicals are synthesized and probed at the same region in the middle of the 6 cm diameter flow tube. Second order fits of the CH_2OO decay traces in the absence of SO_2 do not show significant first order contributions, as exemplified in Fig. 1, because of a small first order contribution relative to the dominant second order CH_2OO loss process. However, non-zero intercept values ($> 500 \text{ s}^{-1}$) were obtained in the pseudo first order analysis at different total pressures, which appear inconsistent with the fits to second order (self-reaction) decays. To resolve this issue, experiments were performed to obtain CH_2OO decay traces in the presence of lower concentrations of SO_2 , more comparable with the CH_2OO concentration.

Fig. 7 shows the CH_2OO decay trace obtained at the lowest SO_2 concentration used in the current work, and the fit using eqn (22) to obtain the first order contribution. Although the pseudo first-order approximation might be expected to break down at the lower end of our SO_2 concentration range, numerical modelling shows that a pseudo first-order treatment remains valid because of the rapidity of the CH_2OO self-reaction. The overall kinetics are still well-described by simultaneous second and first order fits (adjusted $R^2 > 0.99$). The inset in Fig. 7 shows the non-linear behaviour of the plot of the reciprocal of $\Delta\kappa$ as a function of time caused by a first order contribution to the dominant second order decay (CH_2OO self-reaction). Fig. 8 shows the pseudo first order rate coefficients obtained from analysis of the CH_2OO decay traces taken over our whole range of low to high SO_2 concentrations. We see the onset of curvature in the plot for $[\text{SO}_2]$ values that are still in more than four-fold

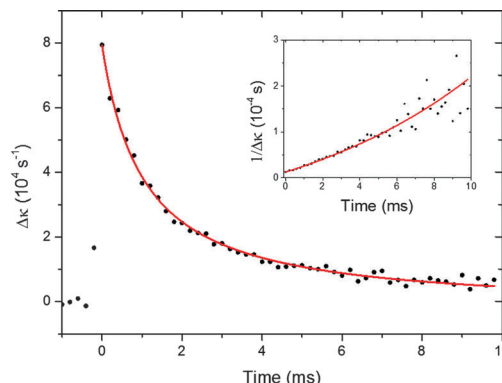


Fig. 7 CH_2OO decay trace obtained in the presence of low $[\text{SO}_2]$ ($1.1 \times 10^{12} \text{ molecule cm}^{-3}$). The initial concentration of CH_2OO was $\sim 4.9 \times 10^{12} \text{ molecule cm}^{-3}$. The solid lines show the fits performed using eqn (22). The inset shows the reciprocal of the experimental and fitted $\Delta\kappa$ values as a function of time for clarity. A first order contribution of $92 \pm 6 \text{ s}^{-1}$ was obtained from this fit.

excess over the initial concentration of CH_2OO . Separate linear fits were performed for the four highest (8.64×10^{13} to $2.16 \times 10^{14} \text{ molecule cm}^{-3}$) and four lowest (1.08×10^{12} to $6.48 \times 10^{12} \text{ molecule cm}^{-3}$) SO_2 concentrations. The linear fit expressions obtained are $(3.93 \pm 0.13) \times 10^{-11} \times [\text{SO}_2] + 629 \pm 147$ and $(7.46 \pm 0.29) \times 10^{-11} \times [\text{SO}_2] + 11.6 \pm 8.0$ for the high and low SO_2 concentration regimes, respectively. Linear Fit 1 gives the $\text{CH}_2\text{OO} + \text{SO}_2$ reaction contribution, whereas Linear Fit 2 suggests a different mechanism also contributes at low SO_2 concentrations.

We hypothesize an SO_2 -catalysed but reversible isomerization or ISC mechanism, in competition with reaction to $\text{HCHO} + \text{SO}_3$, to explain what we see. A generalized kinetic analysis incorporating the idea is presented in the ESI† and accounts for the observed dependence of k_{pseudo} on $[\text{SO}_2]$. Previous theoretical work by Vereecken *et al.* suggests 17% of the $\text{CH}_2\text{OO} + \text{SO}_2$ reaction leads to singlet bisoxy radical + SO_2 *via* a pathway with a submerged energy barrier,³⁰ and this isomerization mechanism is one candidate for our experimental observations. However, we note that the

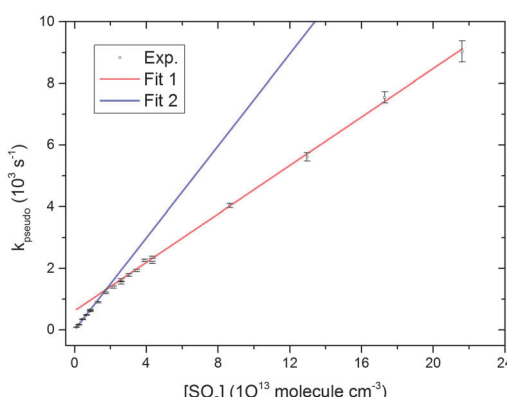


Fig. 8 Pseudo first order rate coefficients as a function of SO_2 concentration. All the decay traces were taken at 10 Torr total pressure. Fit 1 and Fit 2 are the linear fits for the four highest and four lowest SO_2 concentration pseudo first order rate coefficients, respectively.

reversibility of our proposed mechanism conflicts with the calculations of Vereecken *et al.* which place the ground states of isomers of CH_2OO more than 60 kJ mol^{-1} lower in energy than the Criegee intermediate. An alternative candidate is formation of a triplet state species *via* intersystem crossing and the calculations of Vereecken *et al.* lend some support to this suggestion. These authors identified that, in the vicinity of the $\text{OCH}_2\text{OS(O)O}$ biradical adduct of CH_2OO and SO_2 , the singlet and triplet states are split by less than 0.4 kJ mol^{-1} ; at near degeneracy here or elsewhere in the $\text{CH}_2\text{OO} - \text{SO}_2$ configuration space, singlet-triplet mixing may be significant and lead to reversible ISC.

In the absence of an alternative explanation for our experimental observations, we are forced to propose an as-yet unidentified intermediate species such as a triplet biradical, or question the accuracy of the existing calculations, which use single reference methods to describe biradical intermediates that (as the authors themselves argue) would be better treated with multi-reference techniques. Our suggested mechanism remains tentative and clearly is subject to testing if multi-reference electronic structure calculations are performed, or the triplet state reaction pathways are mapped. We therefore do not place undue emphasis on this mechanism here, and further details of our model and analysis instead appear in the ESI.†

The analysis based on our proposed mechanism shows that the pseudo first order rate coefficient at high SO_2 concentration can be attributed to bimolecular reaction of CH_2OO and SO_2 but the intercept of fit 1 depends on both the rate coefficient for unimolecular dissociation of CH_2OO in the absence of SO_2 and that for the intermediate isomer, as well as the ratio of forward and backward isomerization rate coefficients. This analysis is supported by numerical fitting, which is also discussed in the ESI.† The intercept value for Fit 1 does not have significant dependence on total pressure (intercept values at pressures, 10 to 30 Torr, are provided in Table S4 in the ESI†) and a pressure independent value of $704 \pm 47 \text{ s}^{-1}$ was obtained. In the low SO_2 pressure regime, our model indicates that the pseudo first order rate coefficient should be the sum of contributions from bimolecular reaction and catalysed isomerization/ISC by SO_2 , justification for which is provided in the ESI.† A value of $(3.53 \pm 0.32) \times 10^{-11} \text{ cm}^3 \text{ molecule}^{-1} \text{ s}^{-1}$ was obtained for the catalysed isomerization/ISC rate coefficient by subtraction and propagation of errors of the slope values obtained from Fit 1 and Fit 2.

The intercept of the low SO_2 concentration fit (Fit 2), $11.6 \pm 8.0 \text{ s}^{-1}$, is taken as an upper limit for the unimolecular loss of CH_2OO in the absence of SO_2 -induced isomerization/ISC, because it may also contain diffusion and mass flow contributions. Unimolecular rate coefficient values from 100 to 200 s^{-1} have been used previously for atmospheric chemistry modelling of stabilized CH_2OO .³³ These values were taken as an estimated upper limit from laboratory based studies of CH_2OO .⁹ Several recent studies have also reported upper limit estimates for the unimolecular loss rate coefficient around 200 s^{-1} .^{16,26,37} Significant contribution from wall reactions prevented accurate determination of the CH_2OO unimolecular loss rate coefficient. Olzmann *et al.* estimated the CH_2OO unimolecular loss rate to

be 0.33 s^{-1} based on electronic structure calculations, which is much lower than the estimates from previous kinetic studies using direct sources of CH_2OO .⁴² The CH_2OO unimolecular rate coefficient upper limit value obtained in the current study is more in keeping with the theoretical study. The present study therefore shows that a pathway for CH_2OO losses by catalysed isomerization or ISC could bridge the discrepancies between the prior experimental and theoretical estimates.

(IV) Atmospheric implications

SO_2 concentrations of 10^{10} to 10^{11} molecule cm^{-3} have been reported in rural and urban environments, respectively.³⁰ Thus, the $\text{CH}_2\text{OO} + \text{SO}_2$ reaction should be in the low pressure limit (for SO_2 collisions) in these environments and both the proposed isomerization (or ISC) and bimolecular reaction should be important CH_2OO loss pathways. Both of these reactions should also compete with the unimolecular decomposition of CH_2OO . Maximum pseudo first order reaction rate coefficients of 12, 1.3 and 1.4 s^{-1} are calculated for the CH_2OO unimolecular reaction, the hypothesized SO_2 -catalysed CH_2OO isomerization reaction and $\text{CH}_2\text{OO} + \text{SO}_2$ bimolecular reaction using the rate coefficient obtained in this work and a typical atmospheric SO_2 concentration of 3.8×10^{10} molecule cm^{-3} .³⁰ The lower limiting value for the unimolecular reaction rate coefficient of CH_2OO compared with the one used in a previous modelling study³³ should yield a prediction of higher concentration of stabilized CH_2OO in the atmosphere.

The $\text{CH}_2\text{OO} + \text{H}_2\text{O}$ and $\text{CH}_2\text{OO} + (\text{H}_2\text{O})_2$ reactions are expected to be the most important atmospheric CH_2OO loss mechanisms. Pseudo first order reaction rate coefficients for the $\text{CH}_2\text{OO} + \text{H}_2\text{O}$ and $\text{CH}_2\text{OO} + (\text{H}_2\text{O})_2$ reactions could be as high as 36 and 81 s^{-1} based on maximum rate coefficient estimates of 9×10^{-17} and $3 \times 10^{-13} \text{ cm}^3 \text{ molecule}^{-1} \text{ s}^{-1}$ and typical atmospheric concentration of 4×10^{17} and 2.7×10^{14} molecule cm^{-3} for H_2O and $(\text{H}_2\text{O})_2$ respectively.^{12,28,30} Precise measurements of the $\text{CH}_2\text{OO} + \text{H}_2\text{O}$ and $\text{CH}_2\text{OO} + (\text{H}_2\text{O})_2$ reaction rate coefficients are needed for more accurate estimates. The work of Leather *et al.* derived a ratio for $k_6/k_7 = 3.3 \times 10^{17}$ molecule cm^{-3} , and using the upper limit value for k_6 obtained in this work leads to an estimate for $k_7 = 3.5 \times 10^{-17} \text{ cm}^3 \text{ molecule}^{-1} \text{ s}^{-1}$ (with a range of $1.6 \times 10^{-17} \text{ cm}^3 \text{ molecule}^{-1} \text{ s}^{-1}$ based on the uncertainty in k_6 obtained here).⁴³ These estimates for k_7 are smaller but consistent with the work of Stone *et al.*,²⁸ and larger than the values used in various studies to estimate urban, regional and global CI levels.^{3,9,11,12,33} Hence, CI levels in these studies may be underestimated, but caution is needed as the rate coefficient for reaction of CI species with water dimers has come under some scrutiny recently and may be sufficiently large to offset this change. Nevertheless, the possibility of significant levels of CI in the boundary layer in particular are supported by this work.

Conclusions

Rate coefficient values for CH_2OO self-reaction, reaction with SO_2 and unimolecular reaction were obtained at 293 K and



under low pressure (7 to 30 Torr) conditions using cavity ring-down spectroscopy. Rate coefficient values for the CH_2OO self-reaction and reaction with SO_2 obtained in the current study are in agreement with previously reported values obtained by different methods. The rate coefficient value for CH_2OO unimolecular reaction was found to be significantly lower compared to the estimates from previous experimental studies, but in line with a theoretical estimate. Reversible isomerization or intersystem crossing of CH_2OO that is catalysed by SO_2 is proposed to explain the discrepancy between previous experimental estimates and the theoretical calculations.

Acknowledgements

This work was funded by Natural Environment Research Council (NERC) grant NE/K004905/1. We are grateful to Leonid Sheps and Craig Taatjes (Sandia National Laboratory) for valuable discussions.

References

- 1 R. Criegee and G. Wenner, *Liebigs Ann. Chem.*, 1949, **564**, 9–15.
- 2 D. Johnson and G. Martson, *Chem. Soc. Rev.*, 2008, **37**, 699–716.
- 3 C. A. Taatjes, D. E. Shallcross and C. J. Percival, *Phys. Chem. Chem. Phys.*, 2014, **16**, 1704–1718.
- 4 J. G. Calvert, R. Atkinson, J. A. Kerr, S. Madronich, G. K. Moortgat, T. J. Wallington and G. Yarwood, *The mechanisms of atmospheric oxidation of the alkenes*, Oxford University Press, 2000.
- 5 J. H. Kroll, J. S. Clarke, N. M. Donahue, J. G. Anderson and K. L. Demerjian, *J. Phys. Chem. A*, 2001, **105**, 1554–1560.
- 6 J. H. Kroll, S. R. Sahay, J. G. Anderson, K. L. Demerjian and N. M. Donahue, *J. Phys. Chem. A*, 2001, **105**, 4446–4457.
- 7 L. Lu, J. M. Beames and M. I. Lester, *Chem. Phys. Lett.*, 2014, **598**, 23–27.
- 8 C. A. Taatjes, G. Meloni, T. M. Selby, A. J. Trevitt, D. L. Osborn, C. J. Percival and D. E. Shallcross, *J. Am. Chem. Soc.*, 2008, **130**, 11883–11885.
- 9 O. Welz, J. D. Savee, D. L. Osborn, S. S. Vasu, C. J. Percival, D. E. Shallcross and C. A. Taatjes, *Science*, 2012, **335**, 204–207.
- 10 C. A. Taatjes, O. Welz, A. J. Eskola, J. D. Savee, D. L. Osborn, E. P. F. Lee, J. M. Dyke, D. W. K. Mok, D. E. Shallcross and C. J. Percival, *Phys. Chem. Chem. Phys.*, 2012, **14**, 10391–10400.
- 11 C. A. Taatjes, O. Welz, A. J. Eskola, J. D. Savee, A. M. Scheer, D. E. Shallcross, B. Rotavera, E. P. F. Lee, J. M. Dyke, D. L. Osborn, D. M. K. Mok and C. J. Percival, *Science*, 2013, **340**, 177–180.
- 12 O. Welz, A. J. Eskola, L. Sheps, B. Rotavera, J. D. Savee, A. M. Scheer, D. L. Osborn, D. Lowe, A. M. Booth, P. Xiao, M. A. H. Khan, C. J. Percival, D. E. Shallcross and C. A. Taatjes, *Angew. Chem., Int. Ed.*, 2014, **53**, 4547–4550.
- 13 J. M. Beames, F. Liu, L. Lu and M. I. Lester, *J. Am. Chem. Soc.*, 2012, **134**, 20045–20048.
- 14 J. M. Beames, F. Liu, L. Lu and M. I. Lester, *J. Chem. Phys.*, 2013, **138**, 244307.
- 15 J. H. Lehman, H. Li, J. M. Beames and M. I. Lester, *J. Chem. Phys.*, 2013, **139**, 141103.
- 16 L. Sheps, *J. Phys. Chem. Lett.*, 2013, **4**, 4201–4205.
- 17 E. P. F. Lee, D. K. W. Mok, D. E. Shallcross, C. J. Percival, D. L. Osborn, C. A. Taatjes and J. M. Dyke, *Chem. – Eur. J.*, 2012, **18**, 12411–12423.
- 18 W. L. Ting, Y. H. Chen, W. Chao, M. C. Smith and J. J. M. Lin, *Phys. Chem. Chem. Phys.*, 2014, **16**, 4039–4049.
- 19 F. Liu, J. M. Beames, A. M. Green and M. I. Lester, *J. Phys. Chem. A*, 2014, **118**, 2298–2306.
- 20 Y. T. Su, Y. H. Huang, H. A. Witek and Y. P. Lee, *Science*, 2013, **340**, 174–176.
- 21 J. Ahrens, P. T. M. Carlsson, N. Hertl, M. Olzmann, M. Pfeifle, J. L. Wolf and T. Zeuch, *Angew. Chem., Int. Ed.*, 2014, **53**, 715–719.
- 22 M. Nakajima and Y. Endo, *J. Chem. Phys.*, 2013, **139**, 101103.
- 23 M. C. McCarthy, L. Cheng, K. N. Crabtree, O. Martinez, T. L. Nguyen, C. C. Womack and J. F. Stanton, *J. Phys. Chem. Lett.*, 2013, **4**, 4133–4139.
- 24 M. Nakajima and Y. Endo, *J. Chem. Phys.*, 2014, **140**, 134302.
- 25 Z. J. Buras, R. M. I. Elsamra, A. Jalan, J. E. Middaugh and W. H. Green, *J. Phys. Chem. A*, 2014, **118**, 1997–2006.
- 26 Y. Liu, K. D. Bayes and S. P. Sander, *J. Phys. Chem. A*, 2014, **118**, 741–747.
- 27 L. Vereecken, H. Hardera and A. Novellia, *Phys. Chem. Chem. Phys.*, 2014, **16**, 4039–4049.
- 28 D. Stone, M. Blitz, L. Daubney, N. U. M. Howes and P. Seakins, *Phys. Chem. Chem. Phys.*, 2014, **16**, 1139–1149.
- 29 B. Ouyang, M. W. McLeod, R. L. Jones and W. J. Bloss, *Phys. Chem. Chem. Phys.*, 2013, **15**, 17070–17075.
- 30 L. Vereecken, H. Hardera and A. Novelli, *Phys. Chem. Chem. Phys.*, 2012, **14**, 14682–14695.
- 31 R. L. Mauldin-III, T. Berndt, M. Sipila, P. Paasonen, T. Petaja, S. Kim, T. Kurten, F. Stratmann, V. M. Kerminen and M. Kulmala, *Nature*, 2012, **488**, 193–196.
- 32 J. Li, Y. Qi, B. Q. Yi and P. Yang, *Atmos. Environ.*, 2013, **79**, 442–447.
- 33 C. J. Percival, O. Welz, A. J. Eskola, J. D. Savee, D. L. Osborn, D. O. Topping, D. Lowe, S. R. Utembe, A. Bacak, G. McFiggans, M. C. Cooke, P. Xiao, A. T. Archibald, M. E. Jenkin, R. G. Derwent, I. Riipinen, D. W. K. Mok, E. P. F. Lee, J. M. Dyke, C. A. Taatjes and D. E. Shallcross, *Faraday Discuss.*, 2013, **165**, 45–73.
- 34 J. R. Pierce, M. J. Evans, C. E. Scott, S. D. D'Andrea, D. K. Farmer, E. Swietlicki and D. V. Spracklen, *Atmos. Chem. Phys.*, 2013, **13**, 3163–3176.
- 35 Y. T. Su, H. Y. Lin, R. Putikam, H. Matsui, M. C. Lin and Y.-P. Lee, *Nat. Chem.*, 2014, **6**, 477–483.
- 36 C. A. Taatjes, D. E. Shallcross and C. J. Percival, *Nat. Chem.*, 2014, **6**, 461–462.
- 37 Z. J. Buras, R. M. I. Elsamra and W. H. Green, *J. Phys. Chem. Lett.*, 2014, **5**, 2224–2228.
- 38 W.-L. Ting, C.-H. Chang, Y.-F. Lee, H. Matsui, Y.-P. Lee and J. J.-M. Lin, *J. Chem. Phys.*, 2014, **141**, 104308.



39 B. Long, X.-F. Tan, Z.-W. Long, Y.-B. Wang, D. S. Ren and W.-J. Zhang, *J. Phys. Chem. A*, 2011, **115**, 6559–6567.

40 D. L. Baulch, J. Duxbury, S. J. Grant and D. C. Montague, *J. Phys. Chem. Ref. Data*, 1981, **10**, 1–721.

41 J. H. Espenson, *Chemical Kinetics and Reaction Mechanisms*, The McGraw-Hill Companies, Inc, USA, 1995.

42 M. Olzmann, E. Kraka, D. Kremer, R. Gutbrod and S. Andersson, *J. Phys. Chem. A*, 1997, **101**, 9421–9429.

43 K. E. Leather, M. R. McGillen, A. T. Archibald, S. R. Utembe, M. E. Jenkin, R. G. Derwent, M. C. Cooke, D. E. Shallcross and C. J. Percival, *Atmos. Chem. Phys.*, 2012, **12**, 469–479.

